Largescale flows and resonances in 2D thermal convection

J. Prat, J. M. Massaguer, and I. Mercader

Citation: Phys. Fluids **7**, 121 (1995); doi: 10.1063/1.868732
View online: http://dx.doi.org/10.1063/1.868732
View Table of Contents: http://pof.aip.org/resource/1/PHFLE6/v7/i1
Published by the AIP Publishing LLC.

Large-scale flows and resonances in 2-D thermal convection

J. Prat
Departament de Matemàtica Aplicada i Telemàtica, Universitat Politècnica de Catalunya, 08034 Barcelona, Spain

J. M. Massaguer and I. Mercader
Departament de Física Aplicada, Universitat Politècnica de Catalunya, 08034 Barcelona, Spain

(Received 5 October 1993; accepted 14 September 1994)

Recent experiments of thermal convection in finite containers of intermediate and large aspect ratios have shown the presence of flows spanning the largest dimension of the container [R. Krishnamurti and L. N. Howard, Proc. Natl. Acad. Sci. **78**, 1985 (1981); J. Fluid Mech. **170**, 385 (1986)]. Large-scale flows of this kind computed from two-dimensional (2-D) numerical simulations are presented. The marginal stability curves for the bifurcations are computed in the range of aspect ratios $L=1,\ldots,6$ and for Prandtl number $\sigma=10$. The nonlinear dynamics of the bifurcated solution is explored for containers with aspect ratios $L=1,2,4$. By increasing the Rayleigh number from criticality the system produces different sequences of symmetry breaking, Hopf-type bifurcations, which finally result in large scale flows, oscillatory net mass flux and chaos. The bifurcation involves different mode resonances with vertical and horizontal couplings, which are modeled using formal group theoretical techniques. © *1995 American Institute of Physics.*

I. INTRODUCTION

There is experimental evidence showing that thermal convection in a horizontal layer of fluid heated from below can show motions spanning the largest dimension of the container.[1] The experiments were conducted in a large aspect ratio box, thus challenging the widespread confidence that flows in finite containers should scale as its transverse dimension—i.e., the length along the direction of the driving force. Because the experimental setting precluded any externally imposed pressure head or shear stresses, it must be concluded that these large-scale motions were driven by a Reynolds stress tensor with nonzero horizontal average, $\tau_{xz}=\overline{v_x' v_z'}$.

From the theoretical point of view, a finite container is an object that is difficult to handle. Most of the theory for flows in finite containers has been derived for boxes that are periodic in their longitudinal directions. This is a proper idealization for flows in large aspect ratio boxes. If the aspect ratio is large, the solutions obtained for a box with lateral boundaries are expected to show small deviations from solutions in periodic boxes. Lateral boundaries are only expected to introduce small-range perturbations, thus modulating the periodic solution at the far ends of the container. However, the large-scale flows mentioned before are challenging in this respect, and may change such a picture. Getting rid of the boundaries by assuming a horizontally periodic layer may even give rise to flows that cannot be traced back to solutions in a finite container, as is the case for flows with net horizontal mass flux.

The goal of the present paper is to understand large-scale flows in two-dimensional, periodic containers, which we shall call, henceforth, periodic channels. Besides its obvious connections with the Bénard problem, we believe this problem to be important in its own right. Relevant experiments in this respect are those of convection in Hele–Shaw cells. One such experiment, performed in a container of aspect ratio $L\simeq 10$, shows how convection cells can spontaneously tilt, which means that a shearing motion has been destabilized.[2] Such a flow arises because of a mean horizontal velocity field showing an antisymmetric profile, thus shearing the flow. We shall associate the tilting of these cells with the presence of a large-scale flow component.

There is still another experiment of relevance in the present context. It is an experiment on thermal convection in a container of aspect ratio $L=32$ filled with air ($\sigma\simeq 1$).[3] As reported by the authors in a footnote, "Subsequent side views showed that roll-edge tilt angles up to plus/minus ten degrees can occur." The tilting of the cells shows the presence of a large-scale shear flow. In this experiment the tilting was periodic, thus showing periodic flow reversals, in contrast with the steady tilting observed in the Hele–Shaw experiment described above.

The first numerical simulations showing large-scale flows or shear flows, with both names being used as synonyms, were done for convection in a compressible fluid.[4,5] These were open-type flows, driven only by a difference in temperature between top and bottom. Convection in very small aspect ratio containers resulted in very strong shears, but a shear-type flow was also obtained for some intermediate aspect ratio containers. The flows were time dependent, but no flow reversal has been reported. In spite of the small number of cases run, the feeling was that large scale flows may or may not develop, depending on the aspect ratio of the periodic box. Recently, some two-dimensional (2-D) numerical simulations of convection in a small aspect ratio container, $L=1$, filled with a Boussinesq fluid have been done.[6] Motivation came from instabilities observed in plasma physics—in the edge of a tokamak, to be precise—where large-scale flows have also been observed, but no attempt to explore larger aspect ratio dynamics has been reported.

There have been several recent attempts to model such large-scale flows. In two of them[2,7] the nonlinear dynamics was explored by assuming modal truncations that provide a

plausible description for the tilting of the cells. Galerkin-type expansions were assumed, such that parity could spontaneously break in both x and z coordinates, thus making provisions for $\tau_{xz} \neq 0$. Both papers included only one horizontal mode, thus forcing a 1:1 coupling in the horizontal direction. As a consequence, the coupling could drive a $n=0$ mode, the mean velocity field $\mathbf{U}$, which bifurcates from the primary flow by breaking its parity.

A different kind of mechanism that can trigger large-scale flows is that of resonance. Several models have been derived so far, either by using small amplitude expansions or group theoretical methods. If the horizontal length of the container is such that two or more solutions, each one with a different number of cells, fit inside the container, they can be nonlinearly coupled. The so-called 2:1 resonance, which takes place between modes of horizontal wave numbers $k=1,2$ was the first examined.[8,9] These modes couple at cubic order as (2,1,1) and may give rise to a large-scale flow, provided that parity breaks down. More recently the resonances 1:3 and 1:2:3 have also been examined with similar results.[10]

In the following, we shall examine three sets of examples of convection in three 2-D periodic channels of small aspect ratio. In Sec. II we shall derive the equations and numerical techniques. In Sec. III we shall present the numerical results. In Sec. IV we shall derive an amplitude equation that fits the numerical results, and we shall discuss its dynamics. Finally, in Sec. V we shall conclude by summarizing some of the physical implications.

II. EQUATIONS

The purpose of the present paper is to deal with two-dimensional thermal convection in periodic channels under the most general conditions. In order to allow a net mass flux along the channel it is convenient to split the velocity solenoidal field $\mathbf{v}$ between its mean and fluctuating components,

$$\mathbf{v}=\mathbf{U}+\mathbf{v}',$$

where $\mathbf{U}=[U(z,t),0]$, $\mathbf{v}'=(-\partial_z\chi',\partial_x\chi')$ and $\bar{\mathbf{v}}'=\bar{\chi}'=0$, with an overline meaning horizontal average over the periodic domain. With this choice we depart from the most usual formulation of the Bénard problem by allowing a net mass flux, $\int_{-1/2}^{+1/2}U(z,t)dz$. This is mandatory if a formulation in terms of the primitive variables is chosen, but streamfunction formulations are very popular, and the mean mass flux is often killed by assuming the streamfunction to be zero on top and bottom. The temperature will be split as

$$T=1/2-z+T'.$$

Equations for U, χ', and T' can be obtained, respectively, from the horizontal average of the Navier–Stokes equations, the deviation of the vorticity equation from its horizontal average, and the heat equation. By writing them in nondimensional form, we get

$$(\partial_t-\sigma\partial_{zz}^2)U+\partial_z\overline{v_x'v_z'}=0, \tag{1a}$$

$$(\partial_t+U\partial_x-\sigma\nabla^2)\omega'+R\sigma\partial_xT'+\partial_{zz}^2U\partial_x\chi'+\frac{\partial(\chi',\omega')}{\partial(x,z)}-\overline{\frac{\partial(\chi',\omega')}{\partial(x,z)}}=0, \tag{1b}$$

$$(\partial_t+U\partial_x-\nabla^2)T'-\partial_x\chi'+\frac{\partial(\chi',T')}{\partial(x,z)}=0, \tag{1c}$$

where $\omega'=-\nabla^2\chi'$, R is the Rayleigh number, σ is the Prandtl number, time is scaled against the thermal diffusion time, and the equations are defined in the domain $(x,z)\in[0,L]\times[-1/2,+1/2]$. The boundary conditions will be taken to be periodic in x and nonslip, perfectly conducting in z

$$U=\chi'=\partial_z\chi'=T'=0 \quad \text{for } z=\pm 1/2. \tag{2}$$

A nondecaying mean velocity field U requires a nonzero mean Reynolds stress tensor $\tau_{xz}:=\overline{v_x'v_z'}\neq 0$, and that is equivalent to $\overline{\partial_z\chi'\partial_x\chi'}\neq 0$. Whether such a condition will be fullfilled or not depends on the symmetries of the flow.[11] System (1), (2) is invariant against continuous translations, time shifts, and the following two finite symmetries:

$$S_1:(x,z,t)\to(-x,z,t), \quad (U,\chi',T')\to(-U,-\chi',T'), \tag{3}$$

$$S_2:(x,z,t)\to(-x,-z,t), \quad (U,\chi',T')\to(-U,\chi',-T'). \tag{4}$$

In periodic domains, besides continuous translations, finite translations of an integer fraction of the wavelength are important. In particular, a translation of half a wavelength is a relevant transformation because its square, as well as that of S_1 and S_2, is the identity. Thus we introduce the finite translation

$$S_3:(x,z,t)\to(x+\Lambda/2,z,t), \quad (U,\chi',T')\to(U,\chi',T'), \tag{5}$$

where Λ is the wavelength, which we shall assume to be equal to the length of the container, $\Lambda=L$. Translations of any smaller integer fraction of the wavelength have not been found to be of any relevance so far.

The transformations $\{S_1,S_2,S_3\}$ together with their products define a commutative group of steady finite symmetries for (1), (2). The square of every one of these transformations is the identity, and every transformation is its own inverse. However, stacked rolls are not stable solutions at the onset of convection. Therefore, solutions are not expected to be invariant against $S_1\times S_2$, and the largest subgroup of symmetries that a solution can display is defined by the group of symmetries $G:=\{I,S_1,S_2\times S_3,S_1\times S_2\times S_3\}$, where I is the identity. From this subgroup three different branches emerge, each one breaking two of these nontrivial symmetries, but still remaining invariant to their product, the third symmetry. The first branch is that of solutions invariant against S_1, which from (3) gives $U(z,t)=-U(z,t)$, thus implying $U(z,t)=0$. The second branch is made of solutions invariant against $S_2\times S_3$. Then (4) implies $U(z,t)=-U(-z,t)$, from which U is antisymmetric and the mean

mass flux is zero. The third branch is made of solutions invariant against $\{S_1 \times S_2 \times S_3\}$. Their fingerprint is a symmetric mean velocity field $U(z) = U(-z)$.

Once solutions become time dependent, thus breaking time-shift invariance, a new finite symmetry may become of relevance if the solution is time periodic. By using arguments similar to those used to introduce (5), we shall define the finite symmetry

$$S_4 : (x,z,t) \rightarrow (x,z,t+\tau/2), \quad (U,\chi',T') \rightarrow (U,\chi',T'), \tag{6}$$

where τ is the time period.

A. Numerical method

System (1), (2) was solved using a spectral method. The x dependence was expanded using a pseudospectral trigonometric Fourier expansion and for the z dependence a Chebyshev-collocation method was used. Thus the following expansion was assumed for (U,χ',T')

$$U(z_j,t) = \sum_{m=0}^{M} U_m(t) \mathcal{T}_m(2z_j), \tag{7a}$$

$$\chi'(x,z_j,t) = \sum_{n=-N/2}^{N/2} \sum_{m=0}^{M} \chi_{nm}(t) e^{inkx} \mathcal{T}_m(2z_j), \quad n \neq 0, \tag{7b}$$

$$T'(x,z_j,t) = i \sum_{n=-N/2}^{N/2} \sum_{m=0}^{M} T_{nm}(t) e^{inkx} \mathcal{T}_m(2z_j), \tag{7c}$$

where $\mathcal{T}_m$ are the Chebyshev polynomials of order m, and for the collocation we have taken the Gauss–Lobatto points $2z_j = \cos(\pi j/M)$. The boundary conditions for the vorticity have been imposed using a technique discussed elsewhere,[12] and the solution has been advanced in time using an Adams–Bashforth scheme for the nonlinear terms, together with an implicit Euler scheme for the linear ones. As a standard resolution we have taken $N \times M = 24 \times 24$.

III. NUMERICAL RESULTS

In the present paper we shall examine a few solutions of (1), (2) leading to a nonzero mean velocity field. In an attempt to simplify the dynamics we have concentrated on mildly viscous fluids, $\sigma = 10$. At the onset of convection each solution is invariant against the symmetry group G, therefore $U = 0$. But, by increasing the Rayleigh number, solutions belonging to different aspect ratios break different symmetries. We shall first examine in Sec. III A the marginal stability curves for these ruptures of symmetry and afterwards, in Secs. III B, III C, and III D, we shall examine the nonlinear dynamics for the three different families of solutions emerging from the bifurcation of a single pair of rolls.

A. Marginal stability curves

The linear operator is, by construction, invariant against the group G, thus meaning that it commutes with every one of its elements. As a consequence, the linear problem can be broken into a set of problems, each one involving only solutions that are invariant against a given element of symmetry. To be precise, the linear operator can be projected into every invariant subspace of G. These invariant subspaces overlap. It can be seen by inspection that their overlap is given by the set of solutions that are invariant against the full group of symmetries. As a consequence, the space of solutions splits into four subspaces: three of them invariant against one of each three nontrivial elements of G, and the fourth one invariant against the full group. The implication is that the linear problem factorizes into four linear problems, each one acting on one of these invariant subspaces. Thus four different routes to instability are possible, three of which break two nontrivial symmetries at once. The fourth one preserves every spatial symmetry but, as will be shown below, it changes the shape of the cell.

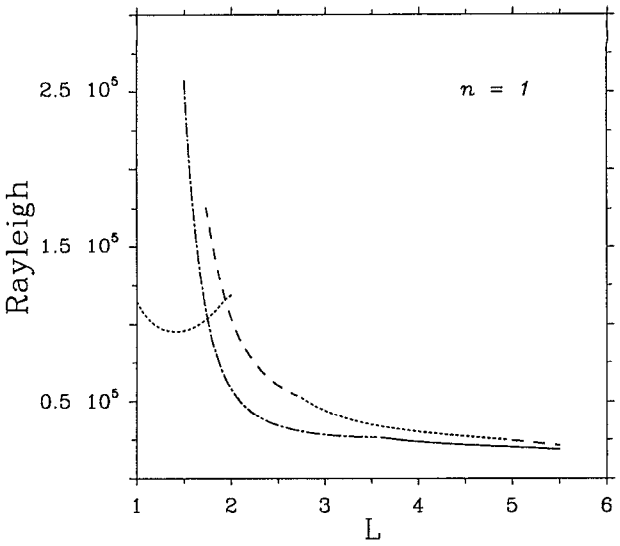

FIG. 1. Rayleigh number R versus aspect ratio L for different states of marginal stability. Every line corresponds to a Hopf bifurcation preserving a different symmetry. There are four different lines, each one corresponding to the four factors of the linear operator. (i) The dotted line designates a bifurcation that preserves $S_2 \times S_3$. It breaks symmetry S_1, thus producing an antisymmetric, nonzero large scale velocity field. (ii) The dashed line designates a rupture of symmetry that preserves symmetry $S_1 \times S_2 \times S_3$. It also breaks S_1, thus still giving a nonzero large-scale velocity field, which is now symmetric. (iii) The dot–dashed line corresponds to a bifurcation that preserves symmetry S_1 but breaks the other two. The mean velocity field is zero. (iv) The solid line designates a Hopf bifurcation preserving all of the symmetries.

In Fig. 1 we have plotted the Rayleigh number as a function of the aspect ratio L for the marginal stability curves of a single pair of rolls. Every curve corresponds to a Hopf bifurcation, and the frequencies have been plotted as a function of the aspect ratios in Fig. 2. All these curves have been computed on the assumption that a single pair of rolls filled the whole domain, and every jump in frequency corresponds to a change in the eigenvalue crossing the real axis, either because a different symmetry becomes dominant, or simply because of a change in the number of nodes of the eigenvalue in either the vertical and the horizontal direction. For aspect ratios smaller than $L \simeq 1.75$ the first instability that sets in preserves the $S_2 \times S_3$ invariance. Therefore, symmetry S_1 is broken and the bifurcated solution displays an

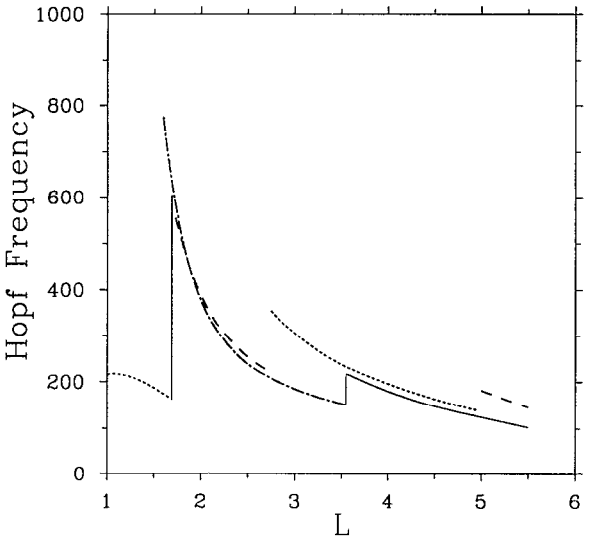

FIG. 2. Frequencies ω versus aspect ratio L for different states of marginal stability. Every line corresponds to a Hopf bifurcation preserving a different symmetry. Lines have been plotted with the same criteria, as in Fig. 1. Every line has only been drawn for the set of L values plotted in Fig. 1. A change in the dominance results in a discontinuity in the Hopf frequency.

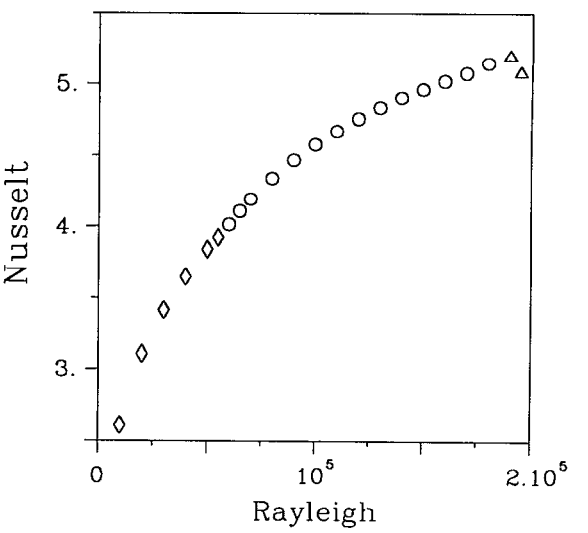

FIG. 3. Nusselt number versus Rayleigh number for periodic solutions in a box of aspect ratio $L=2$. The Prandtl number is $\sigma=10$. Diamonds ($\diamond$) are steady, G-symmetric solutions. Circles (O) are periodic, S_1-symmetric solutions. Triangles ($\triangle$) are chaotic solutions with no symmetry.

antisymmetric nonzero mean velocity field. The corresponding marginal stability curve has been plotted in the figure as a dotted line. For larger values of the aspect ratio the dominant bifurcation is invariant against S_1, thus showing a zero mean velocity field. However, a fairly obvious change in behavior happens at $L\simeq 3.5$, as can be seen from the jump in frequency displayed in Fig. 2. For values of the aspect ratio $1.75<L<3.5$—dot–dashed line—the bifurcated solution preserves S_1 and has broken the other two symmetries in G. In contrast, for $L>3.5$—solid line—the eigenfunction is invariant against the full symmetry group, thus sharing the same spatial symmetries as the unperturbed solution. There are in addition solutions displaying a symmetric profile for U, the bifurcation to which preserves only the symmetry $S_1\times S_2\times S_3$, and the marginal stability curve has been plotted as a dashed line. These solutions have not been found dominant anywhere, as can be seen from Fig. 1. A description of their geometry can be found elsewhere.[13]

In Figs. 1 and 2 we have plotted the marginal stability curves for a single pair of rolls spanning the whole domain, but there are other possibilities. Let us notice that the domain can be filled with several pairs of rolls. An n-pairs solution in a domain of length L can be obtained by replicating n times a pair of rolls fitting a domain of length L/n. Therefore, Fig. 1 can be improved by simply replicating its curves as many times as required. The new solutions will simply be clones. However, the replication brings solutions with a different number of rolls and different symmetries very close. The larger the aspect ratio, the larger the number of solutions for a fixed range of Rayleigh numbers, and the number of possible hybrid solutions increases. Examples of such solutions, also called mixed modes, are well-known results from amplitude type models.[10] Computations in progress show that for aspect ratios larger than $L\simeq 6$, many of such hybrid solutions arise close to the lowest marginal stability curve. We expect them to play an important role on the dynamics in large aspect ratio containers, but a systematic stability analysis in this domain has some technical intricacies, and we shall leave its discussion for a forthcoming paper.

The previous discussion shows that only three different kinds of solutions can bifurcate from a single pair of rolls. We have taken as the prototypes to be examined the containers of aspect ratios $L=1,2,4$. In the following we shall examine the hierarchy of bifurcations and subsequent dynamics that the system undergoes for each of these three aspect ratios.

B. A hierarchy of nonlinear solutions: The case $L=2$

We shall begin by showing solutions in a periodic box of aspect ratio $L=2$, which corresponds to the wave number $k=\pi$, for this value is very close to the critical wave number for convection between rigid boundaries. Figure 3 is a summary of the cases run. By displaying the Nusselt number at $z=1/2$, $N-1:=-\partial_z\tilde{T}'$, as a function of the Rayleigh number we show the three types of solutions found. Above criticality solutions (rhombs) are stationary and G symmetric. At $R=5.9\times 10^4$ the system shows a Hopf bifurcation with frequency $\omega=378$. These new solutions (full circles) break the symmetry $S_2\times S_3$ and $S_1\times S_2\times S_3$, but are still S_1 invariant. A sequence of such solutions, each one a quarter of a period apart has been displayed in Fig. 4. It corresponds to the case $R=8\times 10^4$. The center of the cell bounces periodically against the walls and against the midplane, but preserves reflection symmetry. In addition, broken symmetries $S_1\times S_2\times S_3$ and $S_2\times S_3$ are replaced by $S_1\times S_2\times S_3\times S_4$ and $S_2\times S_3\times S_4$ invariance. The period for this solution is $\tau=2.88\times 10^{-2}$ corresponding to the frequency $\omega=218$.

The dynamics of this wavy motion can be better understood from Fig. 5, where we have plotted the streamfunction

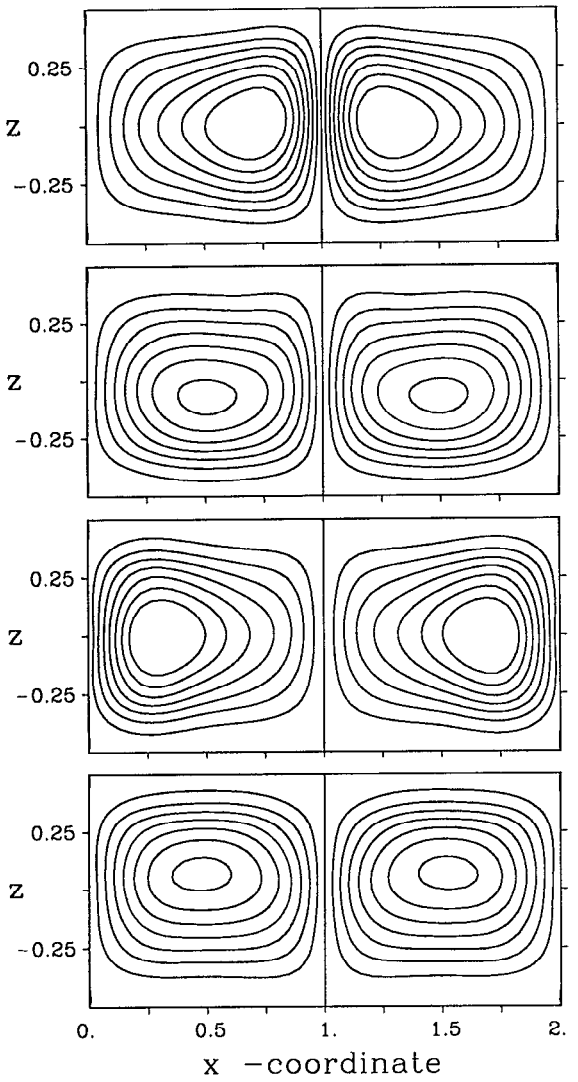

FIG. 4. Streamlines for a sequence of four snapshots a quarter of a period apart each. Aspect ratio $L=2$, Rayleigh number $R=8\times10^4$ and Prandtl number $\sigma=10$. Solutions are S_1 and $S_2\times S_3\times S_4$ symmetric. The period is $\tau=2.88\times10^{-2}$ and the mean flow is zero, $U=0$.

$\chi'(x,t;z=0.25)$ as a 3-D surface. The plot extends for an interval of four periods, and displays the dynamics of a standing wave. The straight line at $x=1$ shows the absence of propagation. Further discussion on its physics will be delayed until the next section.

Around $R\simeq1.9\times10^5$ there is a new bifurcation, now breaking the remaining S_1 symmetry. The bifurcating family of solutions has been plotted in Fig. 3 as triangles. They are chaotic, and this may explain the decrease in the Nusselt number as a result of their reduced coherence. Streamlines, $\chi:=\chi'-\int U\,dz$, for one such a solution, corresponding to $R=1.92\times10^5$, have been plotted in Fig. 6. It can be seen from this figure that not every streamline is closed. Therefore, the mean mass flux is not zero, $\int_{-1/2}^{+1/2} U\,dz\neq0$. This result is consistent with the fact that the symmetry $S_2\times S_3$ had been previously broken. In Fig. 7 we have displayed the mean velocity profile $U(z,t)$ at a fixed time. This profile is certainly not antisymmetric, and the linear momentum of the

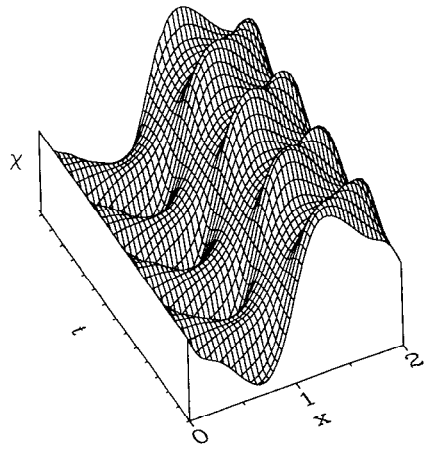

FIG. 5. A surface plot for the streamfunction $\chi'(x,t;z=0.25)$ corresponding to the solution plotted in Fig. 4. The plot extends for an interval of four periods and displays the dynamics of a standing wave.

flow is not conserved. It is transferred back and forth, from and to the wall, by shear stresses.

A time sequence for $U(t;z=0.25)$ is displayed in Fig. 8, showing the reversals of the mean velocity field. The Reynolds number for this velocity, defined as $\mathrm{Re}=U_{\max}/\sigma$ is $\mathrm{Re}\simeq1$, thus showing an important activity. The spectra for $U(t,z=0.25)$ and $\int_{-1/2}^{+1/2} U\,dz$ have been displayed in Figs. 9 and 10, respectively. Both show the broadband spectra characteristic of chaotic solutions, but the two spectra show a very different structure. The transition to chaos has been examined in detail, and takes place by destabilizing an incommensurate frequency. Thus the system reaches chaos through a quasiperiodic regime. The fundamental frequency of the unperturbed solution is $\omega_1=672$, and it bifurcates by giving rise to a new component of frequency $\omega_2=147$. Frequencies have been measured for U. If measured for the Nusselt number ω_2 does not change, but ω_1 doubles its value.

C. A hierarchy of nonlinear solutions: The case $L=1$

In Fig. 11, as a summary of solutions computed for the smaller aspect ratio container $L=1$, we have plotted a Nusselt versus Rayleigh numbers diagram—some preliminary

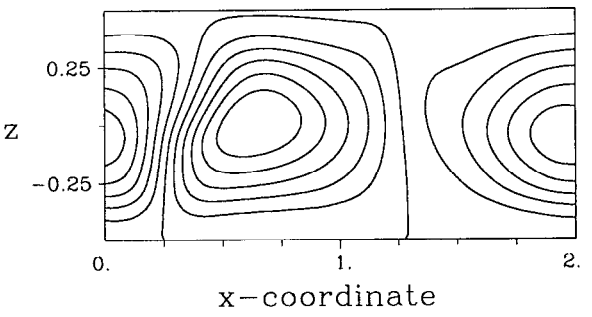

FIG. 6. Streamlines χ for a single snapshot of a chaotic solution. Aspect ratio is $L=2$, Rayleigh number is $R=1.92\times10^5$ and Prandtl number is $\sigma=10$. There is an open streamline, thus showing a nonzero net mass flux, $\int_{-1/2}^{+1/2} U\,dz\neq0$.

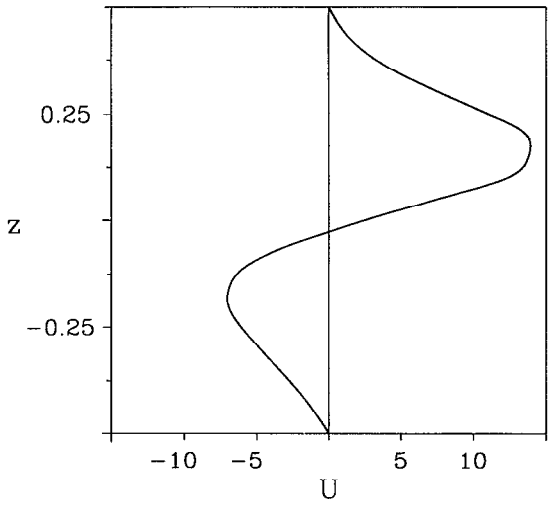

FIG. 7. Mean velocity field U as a function of depth for the chaotic solution displayed in Fig. 6. Aspect ratio is $L=2$, Rayleigh number is $R=1.92\times10^5$ and Prandtl number is $\sigma=10$.

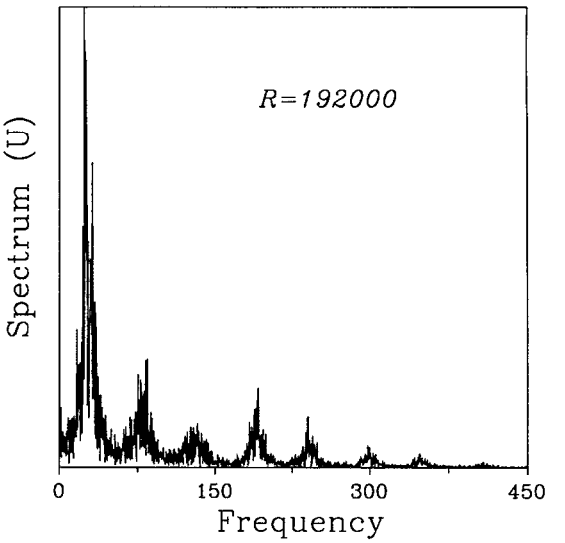

FIG. 9. Fourier spectrum for the mean velocity field $U(z=0.25)$ of the chaotic solution displayed in Fig. 6. Frequency is measured in inverse time units, $f=\omega/2\pi$. Aspect ratio is $L=2$, Rayleigh number is $R=1.92\times10^5$ and Prandtl number is $\sigma=10$.

results can be found elsewhere.[14] The flow is steady and G invariant up to Rayleigh numbers $R\simeq1.15\times10^5$ (rhombs) where it bifurcates to an oscillatory regime with nonzero mean velocity. This is a Hopf bifurcation with frequency $\omega=216$ and the solutions (full circles) break symmetries S_1 and $S_1\times S_2\times S_3$ as required for $U\neq0$, but still preserve $S_2\times S_3$ invariance. An example of such a new solution can be found in Fig. 12, where we have plotted a sequence of snapshots for the streamlines at $R=2\times10^5$ a quarter of a period apart each. The streamlines tilt back and forth at a period $\tau=3.3\times10^{-2}$, corresponding to $\omega=190$, as they shrink and expand at the same pace. The mean velocity field has been displayed in Fig. 13. It is antisymmetric, consistent with the solution being $S_2\times S_3$ invariant, and changes sign by a shrinking to zero and subsequent expansion. The Reynolds number is now Re$\simeq$4, showing a great activity. As in the previous case, broken S_1 and $S_1\times S_2\times S_3$ symmetries have been turned into $S_1\times S_4$ and $S_1\times S_2\times S_3\times S_4$ invariances.

The dynamics of this solution can be better understood from Fig. 14, where we have plotted a 3-D surface for the streamline $\chi(x,t;z=0.25)$. At first sight it may be confusing to decide whether this is a standing wave or a traveling wave, as there is no permanent line of ridges, troughs, or nodes. The three-dimensional (3-D) surface clearly shows the ridges

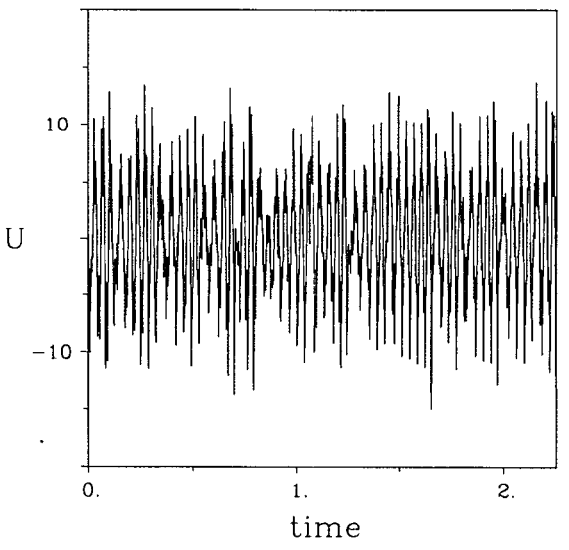

FIG. 8. Mean velocity field $U(z=0.25)$ as a function of time for the chaotic solution displayed in Fig. 6. Aspect ratio is $L=2$, Rayleigh number is $R=1.92\times10^5$ and Prandtl number is $\sigma=10$.

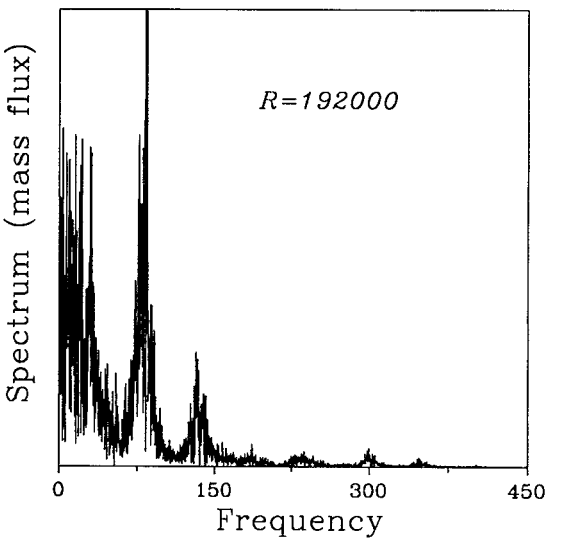

FIG. 10. Fourier spectrum for the net mass flux $\int_{-1/2}^{+1/2} U\,dz$ in the chaotic solution displayed in Fig. 6. Frequency is measured in inverse time units, $f=\omega/2\pi$. Aspect ratio is $L=2$, Rayleigh number is $R=1.92\times10^5$ and Prandtl number is $\sigma=10$.

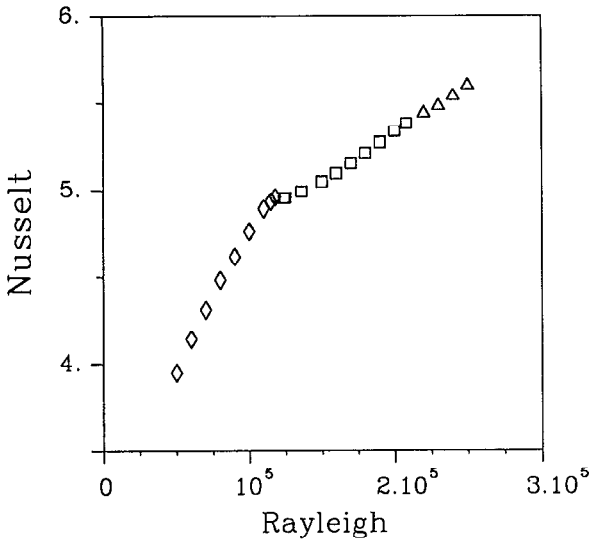

FIG. 11. Nusselt number versus Rayleigh number for periodic solutions in a box of aspect ratio $L=1$. The Prandtl number is $\sigma=10$. Diamonds ($\diamond$) are steady, G-symmetric solutions. Squares ($\square$) are periodic, $S_2\times S_3$-symmetric solutions. Triangles ($\triangle$) are chaotic solutions with no symmetry.

to drift in time back and forth, which might suggest that this a reversing traveling wave.[15] However, the phase velocity does not change sign for all the x simultaneously, as it corresponds to the example of reversing traveling waves. Reflection symmetry is broken, but that is not enough to make a decision about the nature of the wave. We shall go into more detail in the next section.

At $R=2.05\times10^5$ the system reaches a chaotic regime by breaking the remaining $S_2\times S_3$ symmetry (triangles in Fig. 11). As a consequence the mean velocity field U is not antisymmetric anymore, some streamlines are open, and there is a nonzero mean mass flux. A snapshot of the streamlines for the solution $R=2.2\times10^5$ has been plotted in Fig. 15, from which it can be realized that some streamlines do not close. In Fig. 16 we have plotted the mean velocity field at a fixed time for this solution. A slight asymmetry can be easily seen. As in the previous case, the transition to chaos takes place via a quasiperiodic regime. At $R=2.07\times10^5$ leading frequencies are $\omega_1=202$ and $\omega_2=36.4$ for the unperturbed and bifurcated components, respectively, as computed from the U spectra. Some more detail on these spectra can be found elsewhere.[14]

D. A hierarchy of nonlinear solutions: The case $L=4$

We have also examined solutions for the aspect ratio $L=4$. At $R=2.3\times10^4$ a pair of rolls shows a Hopf bifurcation preserving the full group of symmetries G. The frequency is $\omega=180$. One example of such a bifurcated family of solutions, that for $R=2.4\times10^4$, has been displayed in Fig. 17. A sequence of four snapshots, a quarter of period apart each, shows how the streamlines preserve the full group of symmetries. The geometrical difference from the unperturbed roll pair is apparent. The streamlines in the two central snapshots show the presence of the first horizontal overtone as a set of four extrema at midheight. The solutions

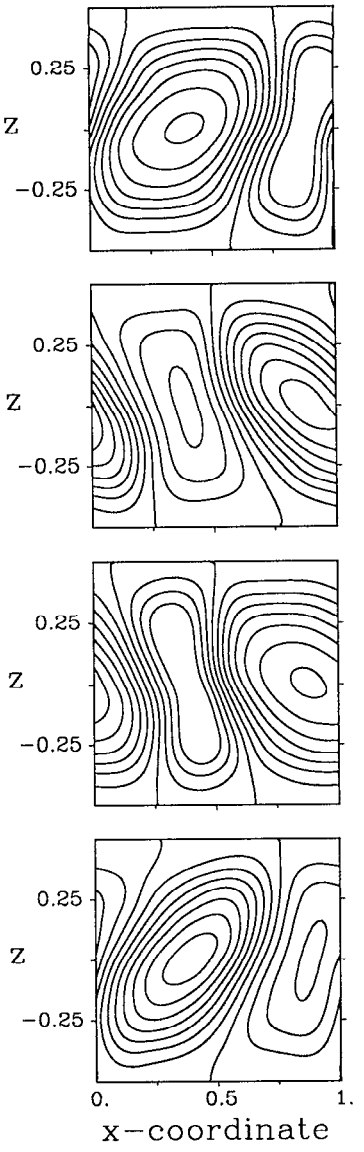

FIG. 12. Streamlines χ for a sequence of four snapshots a quarter of a period apart each. Aspect ratio is $L=1$, Rayleigh number is $R=2\times10^5$, Prandtl number $\sigma=10$. Solutions are $S_1\times S_4$ and $S_2\times S_3$ symmetric. The period is $\tau=3.3\times10^{-2}$ and the mean flow is different from zero, $U\neq0$.

are S_1 invariant and the mean velocity field is zero. However, as in the previous two cases examined, by increasing the Rayleigh number the solution becomes chaotic, and S_1 invariance breaks down, thus resulting in a nonzero mean velocity field U. The corresponding mean mass flux becomes different from zero $\int U\,dz\neq0$. Chaos arises at $R=4.3\times10^4$. A short-time sequence for a chaotic solution at $R=4.5\times10^4$ has been plotted in Fig. 18, where we have plotted $U(z=0.25,t)$. In this figure we have marked the four equally separated instants of time at which we have taken the snapshots displayed in Fig. 19. We have been very careful to display a time interval well within the chaotic regime, and the solutions show the expected lack of symmetries. In contrast with the two previous cases, this time the transition to chaos takes place via a period doubling bifurcation. A window of period three has also been observed near the onset of chaos.

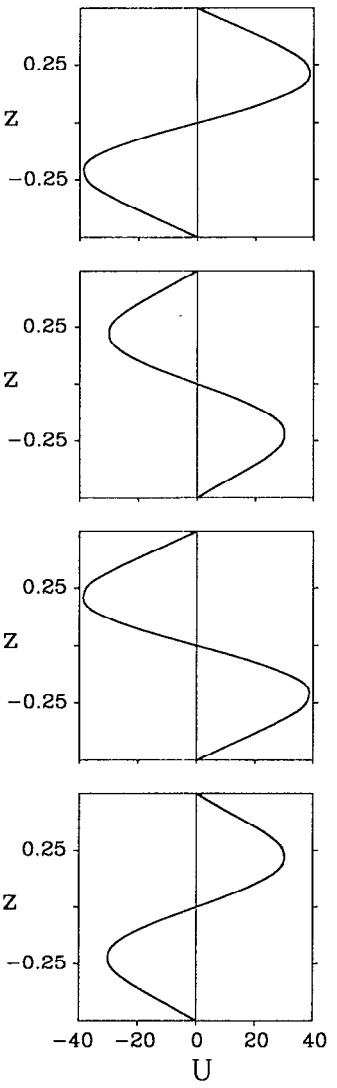

FIG. 13. Mean velocity field U as a function of depth for the sequence of four snapshots displayed in Fig. 12. Aspect ratio $L=1$, Rayleigh number $R=2\times10^5$ and Prandtl number $\sigma=10$. Solutions are $S_1\times S_4$ and $S_2\times S_3$ symmetric. The period is $\tau=3.3\times10^{-2}$.

IV. DISCUSSION

In the previous section we examined 2-D convection in periodic channels of aspect ratios $L=1,2,4$. When the Rayleigh number was increased, the solutions evolved from the most symmetric state, the conduction state, to a state with no spatial symmetry. A mean velocity field with nonzero mass flux has been found in each case to be the result of this lack of spatial symmetry, and the final state has always been found to be chaotic in time. It is worth noticing that every one of these chaotic states displays some memory of previous symmetries. Spatiotemporal symmetries may well be present, but no systematic attempt has yet been made at their description.

The tilting of the cells described in Sec. III C for $L=1$ is consistent with a double mode bifurcation with parity broken in the vertical direction of the kind described in,[2] but the numerical work reported there does not support a Hopf bifurcation to $U\neq0$. Resonances can also result in tilted cells, mean flows and waves,[8–10] but the stability of these flows is not yet completely settled. In addition, bifurcations are not of Hopf type. Both models will be reviewed in Secs. IV A and B, as they are so far the only ones giving a nonzero mean flow. In order to understand the dynamics of our 2-D numerical simulation we shall proceed with a formal derivation.[16,17] The starting point will be the linear stability analysis done in Sec. III B.

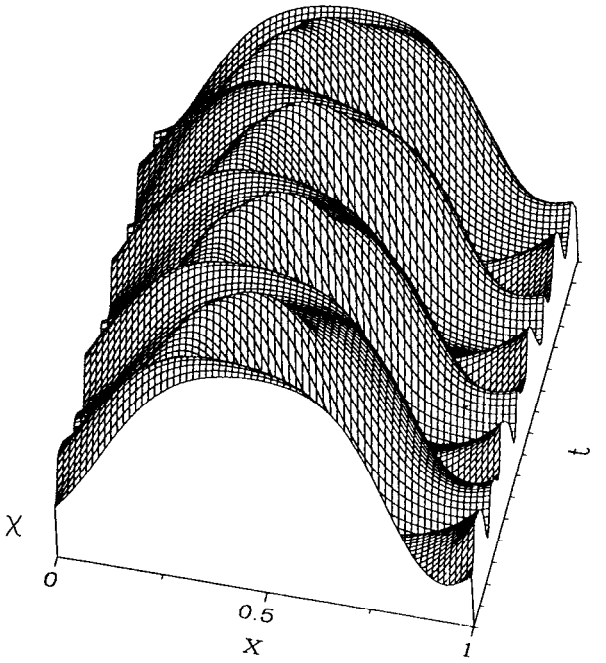

FIG. 14. A surface plot for the streamfunction $\chi(x,t;z=0.25)$ plotted in Fig. 12. The plot extends for an interval of four periods. The contour level at midheight oscillates back and forth in time.

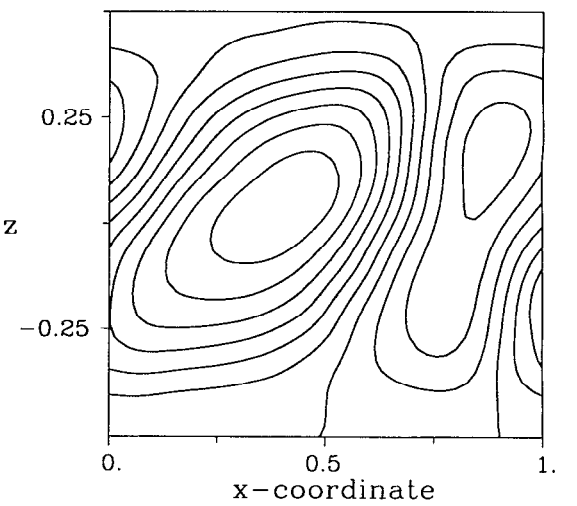

FIG. 15. Snapshot showing the streamlines at a fixed time for a solution with aspect ratio $L=1$, Rayleigh number $R=2.2\times10^5$ and Prandtl number $\sigma=10$. The solution is chaotic and has broken every spatial symmetry. This solution shows a net mass flux.

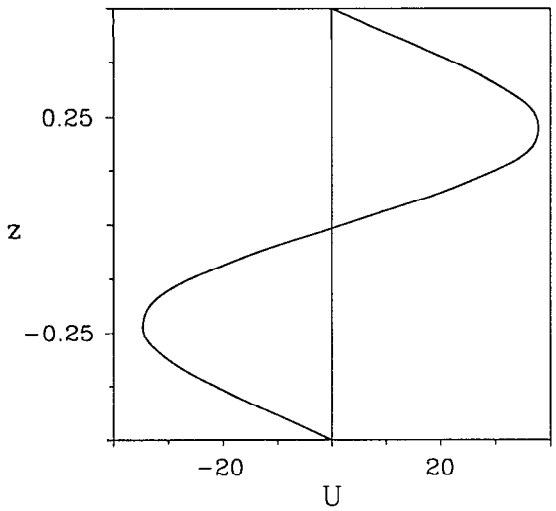

FIG. 16. Mean velocity field U as a function of depth at a fixed time for the solution displayed in Fig. 15. Aspect ratio $L=1$, Rayleigh number $R=2.2\times10^5$ and Prandtl number $\sigma=10$. The solution is chaotic and has broken every spatial symmetry. There is a net mass flux as a result of the slight asymmetry that can be seen in the figure.

The equations that we shall derive are meant to model the dynamics of the physical system as observed from the numerical computations. Although the system will be derived by using a technique that, strictly speaking, is valid only in the asymptotic limit of small amplitude, it will prove to be extremely useful in order to understand the dynamics. In particular, we shall use the model as a diagnostic tool for our numerical results. The number of active degrees of freedom is very small, and therefore the dynamics can be cross-checked with the numerical results. For simplicity we shall refer the whole discussion to the temperature field, T', since this is a scalar field as opposed to the streamfunction, χ', which is a pseudoscalar—i.e., the sign reverses under reflection of the coordinates system. The equations that we shall derive below could be obtained for both fields, but the formulation is simpler for the former than for the latter.

A. Two modes with vertical coupling

Let us begin by assuming for the temperature the following expansion, which generalizes the model derived by Howard and Krishnamurti:[2]

$$T'=(A_1e^{ikx}+\bar{A}_1e^{-ikx})C(z)+(A_2e^{ikx}+\bar{A}_2e^{-ikx})S(z)+\cdots,$$

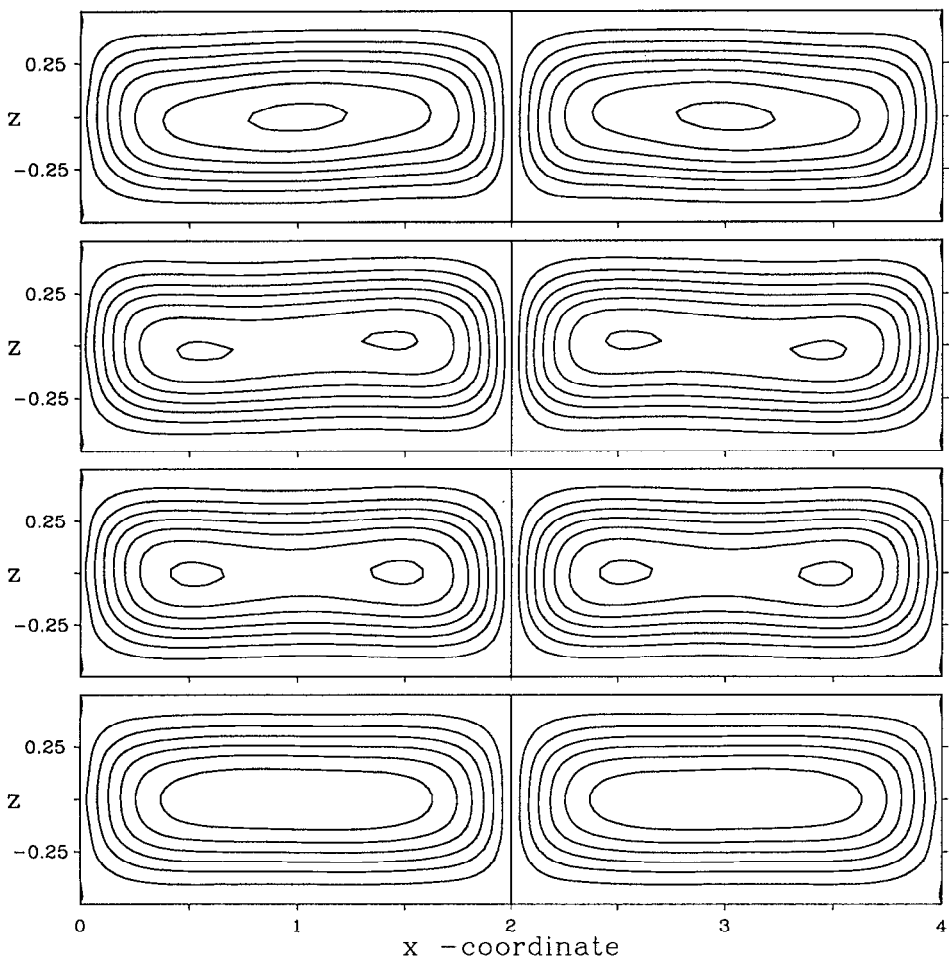

FIG. 17. Streamlines χ for a sequence of four snapshots a quarter of a period apart each. Aspect ratio is $L=4$, Rayleigh number is $R=2.4\times10^4$, Prandtl number $\sigma=10$. Solutions are invariant against the full group of symmetries G. The set of four extrema at midheight in the two central snapshots identifies the activity of the two first overtones as coupled modes. The period is $\tau=3.4\times10^{-2}$, corresponding to $\omega=185$ and the mean flow is zero, $U=0$.

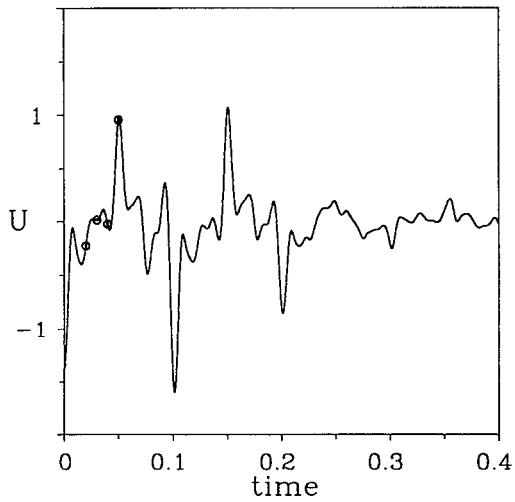

FIG. 18. Time sequence for the mean velocity field $U(z=0.25,t)$ of a chaotic solution. Aspect ratio is $L=4$, Rayleigh number is $R=4.5\times10^4$, Prandtl number $\sigma=10$. The mean velocity field does not show a defined parity and there is a net mass flux. Some indications about the spatial structure can be obtained from Fig. 19, in which we have plotted the streamlines for four snapshots corresponding to the open circles ⊙.

(8)

where $A_j = \rho_j e^{i\xi_j}$, $j=1,2$ are complex amplitudes, $\{C(z),S(z)\}$ are the symmetric and antisymmetric vertical eigenfunctions for the linearized convection problem, with an overline denoting complex conjugates, and higher-order terms are nonlinearly generated, say, by a small-amplitude perturbation technique.

Let us notice that we are dealing with a secondary bifurcation, which may or may not be the unfolding of a multiple bifurcation at the conduction state—i.e., that by a convenient choice of the parameters the bifurcation can be traced back to the conduction state. Unpublished numerical results obtained by using a Galerkin-type model described elsewhere[7] suggest that (8) might bifurcate from the conduction state in the limit of zero Prandtl number. But because the limit $\sigma=0$ is a singular limit, this issue has not yet been systematically pursued. We shall assume (8) with no proof and proceed formally, with no explicit derivation of any coefficients in the amplitude equation.

Amplitudes in (8) should obey a system of equations $\dot{A}_j=f_j(A_1,A_2)$, $j=1,2$ where the $\{f_j\}$ are complex analytic functions. This system of equations has to be invariant

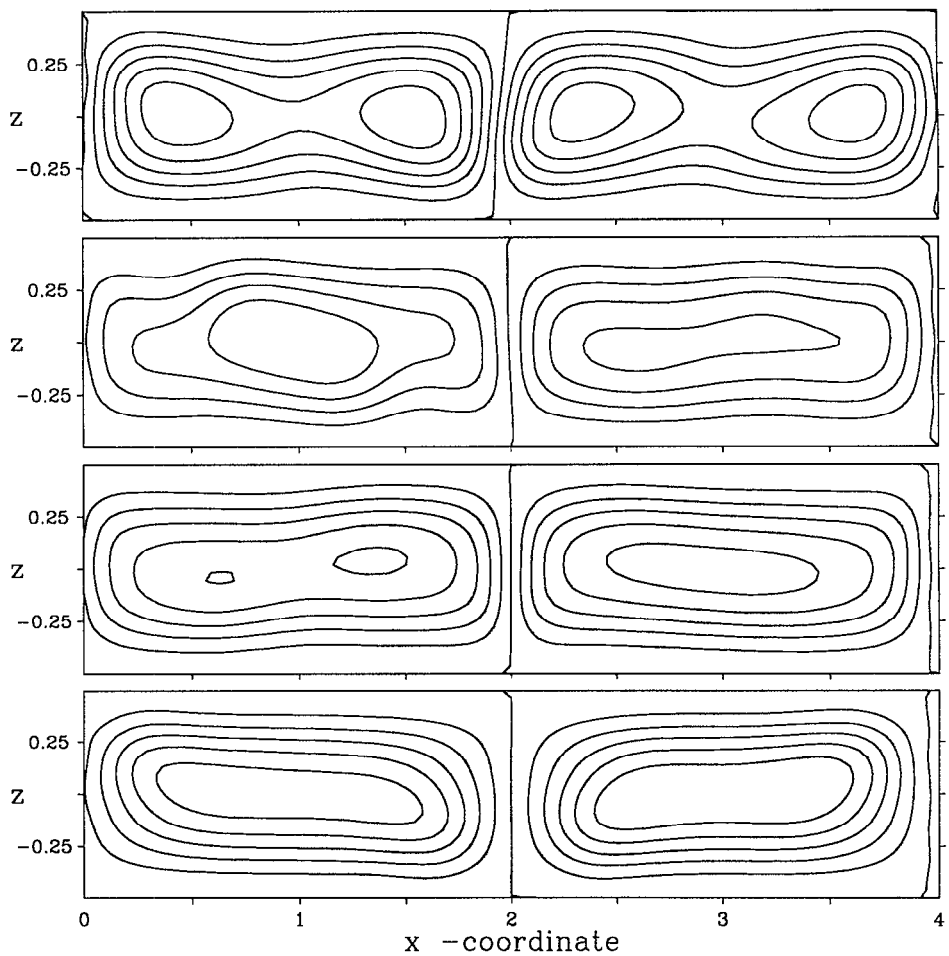

FIG. 19. Streamlines χ for the four snapshots displayed as open circles ⊙ in Fig. 17. Aspect ratio is $L=4$, Rayleigh number is $R=4.5\times10^4$, Prandtl number $\sigma=10$. Snapshots are taken at equal time intervals $\Delta=0.01$. The solution has broken every spatial symmetry, but there is no indication of the cells being tilted in any way. The mean flow and the mass flux are both different from zero.

against continuous translations, as well as invariant against the group G. The action of these transformations on the amplitudes is as follows. A translation will result in the action

$$\tau(x_0):\ A_j e^{ikx} \to A_j e^{ik(x+x_0)}, \quad j=1,2, \tag{9}$$

from where $\tau: A_j \to A_j \exp i\xi_0$, with $\xi_0 = kx_0$. Therefore,

$$\tau: (\rho_j, \xi_j) \to (\rho_j, \xi_j + \xi_0) \tag{10}$$

while symmetries S_1 and $S_2 \times S_3$ result in the actions

$$S_1: (A_1, A_2) \to (\bar{A}_1, \bar{A}_2), \tag{11}$$

$$S_2 \times S_3: (A_1, A_2) \to (\bar{A}_1, -\bar{A}_2). \tag{12}$$

The most general system invariant against transformations (9)–(12) is

$$\dot{A}_1 = \alpha_1 A_1 + \beta_1 \bar{A}_1 A_2^2 + O(|A|^4), \tag{13a}$$

$$\dot{A}_2 = \alpha_2 A_2 + \beta_2 A_1^2 \bar{A}_2 + O(|A|^4), \tag{13b}$$

where $\alpha_j = \alpha_{j0} + \alpha_{j1}|A_1|^2 + \alpha_{j2}|A_2|^2$, $\alpha_{10} > 0$, $\alpha_{11} < 0$ and every coefficient in (13) is real.

Let us assume that a steady solution $\{A_1 = A_0, A_2 = 0\}$ bifurcates from the conduction state. Then $\alpha_{10} + \alpha_{11}|A_0|^2 = 0$. The stability of this solution splits into two equations, one for each amplitude. If $\alpha_{11} < 0$ as is the case, $A_1 \to A_0$, and the equation for A_2 is

$$\dot{A}_2 = (\alpha_{20} + \alpha_{21}|A_0|^2) A_2 + \beta_2 A_0^2 \bar{A}_2. \tag{14}$$

By taking $A_j = x_j + iy_j$ in (14) with x and y real, it is fairly simple to prove that the eigenvalue problem is symmetric, the eigenvalues are real, and the bifurcation is always stationary. Therefore, (13) cannot describe any of the bifurcations previously shown. As a complementary test, we have done explicit numerical computations by using a modal expansion with nonslip boundaries,[7] and the bifurcation has always been found to be steady.

B. Two-mode resonance

The second candidate known to destabilize mean flows is a two-mode resonance, i.e., a double bifurcation with horizontal coupling. We shall now assume for the expansion

$$T' = (A_1 e^{ikx} + \bar{A}_1 e^{-ikx}) C(z) + (A_2 e^{2ikx} + \bar{A}_2 e^{-2ikx}) C(z) + \cdots \tag{15}$$

with $\{A_j = \rho_j \exp i\xi_j\}$. From (15) a continuous translation results in the action

$$\tau: (A_1, A_2) \to (A_1 \exp i\vartheta, A_2 \exp 2i\vartheta) \tag{16}$$

and the action of finite symmetries S_1 and $S_2 \times S_3$ is still given by (11), (12).

The most general system invariant against (11), (12) and (16) can be written as

$$\dot{A}_1 = \alpha_1 A_1 + \beta_1 \bar{A}_1^3 A_2^2 + O(|A|^6), \tag{17a}$$

$$\dot{A}_2 = \alpha_2 A_2 + \beta_2 A_1^4 \bar{A}_2 + O(|A|^6), \tag{17b}$$

where $\alpha_j = \alpha_j(|A_1|^2, |A_2|^2)$. This system was first derived for the analysis of the 2:1 resonance,[9] and the reader should address the original paper for a thorough discussion. A straightforward analysis similar to that done in Sec. IV A shows that the solution $\{A_1 = A_0, A_2 = 0\}$ cannot display a Hopf bifurcation.

C. A system displaying the full group of invariances

Neither of the double mode bifurcations discussed above produces the Hopf bifurcation expected from our numerical results. The implication is that neither of these models describes the marginal stability curves plotted in Fig. 1. A more systematic approach will begin by Fourier expanding T' up to the order where every bifurcation breaking symmetry is allowed. Let us write

$$T' = (A_1 e^{ikx} + \bar{A}_1 e^{-ikx}) C_1(z) + (A_2 e^{ikx} + \bar{A}_2 e^{-ikx}) S_1(z) + (A_3 e^{2ikx} + \bar{A}_3 e^{-2ikx}) C_2(z) + (A_4 e^{2ikx} + \bar{A}_4 e^{-2ikx}) S_2(z) + \cdots, \tag{18}$$

where $\{C_j(z)\}$ and $\{S_j(z)\}$, $j=1,2$ are even and odd functions, respectively, fulfilling the boundary conditions.

The expansion (18) includes the three different components in (8) and (15) plus a fourth one, that of A_4, included for consistency. It will be shown below that this is the minimal set of amplitudes required to describe the four marginal stability curves in Fig. 1. The expectation, supported by the numerical computations, is that any other term that could be included in (18) can be nonlinearly generated. Guidance in this choice has been provided by inspection of the linear operator which, as mentioned in Sec. III A, can be factorized as a product of four different operators, three of them invariant against a nontrivial element of the symmetry group G, and the fourth invariant against the full group.

The action of each symmetry can be derived as in the previous cases. It reads

$$S_1: (A_1, A_2, A_3, A_4) \to (\bar{A}_1, \bar{A}_2, \bar{A}_3, \bar{A}_4), \tag{19}$$

$$S_2 \times S_3: (A_1, A_2, A_3, A_4) \to (\bar{A}_1, -\bar{A}_2, -\bar{A}_3, \bar{A}_4), \tag{20}$$

$$S_1 \times S_2 \times S_3: (A_1, A_2, A_3, A_4) \to (A_1, -A_2, -A_3, A_4). \tag{21}$$

In order to derive the dynamic equation, we shall begin by writing the fundamental translation invariants. They are $\{u_j = |A_j|^2, j=1,\ldots,4\}$, $u_5 = A_1^2 \bar{A}_4$, $u_6 = A_2^2 \bar{A}_4$, $u_7 = A_1 A_2 \bar{A}_3$, $u_1^* = A_1 \bar{A}_2$, $u_2^* = A_3 \bar{A}_4$, $u_3^* = A_1^2 \bar{A}_3$, $u_4^* = A_2^2 \bar{A}_3$, $u_5^* = A_1 A_2 \bar{A}_4$ and their complex conjugates $\{\bar{u}_j, j=1,\ldots,7\}$ and $\{\bar{u}_j^*, j=1,\ldots,5\}$, where we have denoted with an asterisk the invariants changing sign against symmetry (21). Now, the most general system invariant against translations and the group G of discrete symmetries can be written as

$$\dot{A}_1 = \alpha_1 A_1 + \beta_1 A_4 \bar{A}_1 + \gamma_1 A_3 \bar{A}_2 + \alpha_1^* A_2 + \beta_1^* A_3 \bar{A}_1 + \gamma_1^* A_4 \bar{A}_2, \tag{22a}$$

$$\dot{A}_2 = \alpha_2 A_2 + \beta_2 A_4 \bar{A}_2 + \gamma_2 A_3 \bar{A}_1 + \alpha_2^* A_1 + \beta_2^* A_3 \bar{A}_2 + \gamma_2^* A_4 \bar{A}_1, \tag{22b}$$

$$\dot{A}_3 = \alpha_3 A_3 + \beta_3 A_1 A_2 + \alpha_3^* A_4 + \beta_3^* A_1^2 + \gamma_3^* A_2^2, \tag{22c}$$

$$\dot{A}_4 = \alpha_4 A_4 + \beta_4 A_1^2 + \gamma_4 A_2^2 + \alpha_4^* A_3 + \beta_4^* A_1 A_2, \tag{22d}$$

where the coefficients $\{\alpha_j, \beta_j, \gamma_j, j=1,\ldots,4\}$ are functions of the invariants, which are even against transformation (21). The coefficients $\{\alpha_j^*, \beta_j^*, \gamma_j^*, j=1,\ldots,4\}$ are also functions of the invariants, but they are odd against transformation (21). Therefore, the terms with a starred coefficient are at least fourth order in the amplitudes. Symmetry (19), which constrains the constant coefficients in the final expression of (22) to be real, has also to be imposed.

System (22) accepts a steady, roll-type solution $\{A_1=A_0, A_j=0, j=1,2,3\}$. The remaining linear problem for $\{A_1 = A_0 + A_1', A_j = A_j', j=1,2,3\}$ is best written as a function of the translation invariants $\{v_j = A_j'\bar{A}_0, j=1,2\}$ and $\{v_j = A_j'\bar{A}_0^2, j=3,4\}$. It splits into two separate systems. The first one is

$$\dot{v}_1 = a_1 v_1 + b_1|A_0|^2\bar{v}_1 + c_1 v_4 + d_1|A_0|^2\bar{v}_4, \tag{23a}$$

$$\dot{v}_4 = a_4|A_0|^2 v_1 + b_4|A_0|^4\bar{v}_1 + c_4 v_4 + d_4|A_0|^4\bar{v}_4, \tag{23b}$$

and the second one

$$\dot{v}_2 = a_2 v_2 + b_2|A_0|^2\bar{v}_2 + c_2 v_3 + d_2|A_0|^2\bar{v}_3, \tag{24a}$$

$$\dot{v}_3 = a_3|A_0|^2 v_2 + b_3|A_0|^4\bar{v}_2 + c_3 v_3 + d_3|A_0|^4\bar{v}_3. \tag{24b}$$

Every coefficient is now a real constant. The splitting of the linear problem into (23) and (24) is a fairly obvious consequence of symmetry (21).

The eigenvalue problems (23) and (24) can better be solved by using the definition $v_j = x_j + iy_j$. Subsequent separation of real and imaginary parts breaks every system into four independent linear problems for $\{x_1,x_4\}$, $\{y_1,y_4\}$, $\{x_2,x_3\}$ and $\{y_2,y_3\}$. Therefore, the characteristic equations factorize. As a result we get a set of four different characteristic equations

$$(\lambda^2 - \lambda\Gamma_j + \Omega_j) = 0, \quad j=1,\ldots,4. \tag{25}$$

The lines $\Gamma_j = 0$ define the curves of marginal stability for Hopf bifurcations, and the frequencies are given by $\omega^2 = \Omega_j > 0$. The system may also display a stationary bifurcation across the curves of marginal stability $\Omega_j = 0$, if this condition is fulfilled anywhere.

Therefore, because of the factorization, there exist four different families of eigenvalues for (23) and (24), each one associated with a different marginal stability curve: $C_1 := \{x_1,x_4;\ x_2=x_3=y_j=0\}$, $C_2 := \{y_1,y_4;\ y_2=y_3=x_j=0\}$, $C_3 := \{x_2,x_3;\ x_1=x_4=y_j=0\}$, and $C_4 := \{y_2,y_3;\ y_1=y_4=x_j=0\}$. By inspection of (19)–(21) it can be seen that C_1 preserves the full group G of symmetries, but C_2, C_3, or C_4 only preserve a single symmetry. The preserved symmetries are S_1, $S_1\times S_2\times S_3$ and $S_2\times S_3$, respectively.

Now it is clear that the set of amplitudes (18) is minimal. All these amplitudes are required so as to span the four subspaces C_j. But in addition, the previous analysis shows that every one of these eigenmodes couples two different amplitudes, thus being a resonant solution. These resonances between an unperturbed pair of rolls of wave number k and two modes of wave numbers k and $2k$ can be termed (1:1:2) resonances. If we had taken as the unperturbed solution n pairs of rolls, we would have obtained the resonance $(n:n:2n)$, but solutions with n and m pairs can also resonate. This is the case, for instance, for a box with $L=6$, where either a single pair or a triple pair of rolls can fit. The previously discussed resonances are then (1:1:2) and (3:3:6), but they can still couple as a (1:2:3) resonance—see Fig. 1. A few examples of such a resonance have been found, and are currently under study. The presence of such additional resonances increases the number of marginal stability curves, which makes the dynamics very complicated.

As mentioned before, the phase of the roll A_0 is a neutral mode for the linear solutions. Its post-bifurcation behavior can be obtained from the nonlinear terms in (22a). For simplicity in the presentation we shall split the problem into two parts. In the span of the eigenspace $A_1' = A_4' = 0$, we can write (22a) as

$$\dot{A}_1 = \alpha A_1 + \beta A_3\bar{A}_2 + \gamma\bar{A}_1 A_2^2 + \eta A_2 A_3\bar{A}_1^2 + \zeta A_1^2 A_2\bar{A}_3 + \mu A_2^3\bar{A}_3 + O(|A|^5), \tag{26}$$

where the coefficients are functions of the invariants $|A_j|^2$, $j=0,2,3$. We have truncated the equation at fifth order in the amplitudes just to show the leading terms in the expansion, but the reader is to be aware that the truncation should be taken around a finite amplitude solution, and (26) is not a consistent truncation around this point.

Because $A_0 = A_1$, we can now write $A_1 = |A_0|\exp i\xi_0$ and define $\dot{\varphi} := \dot{A}_1\bar{A}_1 - A_1\dot{\bar{A}}_1 = 2i|A_0|^2\dot{\xi}_0$. Then, from (26),

$$\dot{\varphi} = (\beta|A_0|^{-2} - \zeta)(v_3\bar{v}_2 - \bar{v}_3 v_2) + \eta(v_2 v_3 - \bar{v}_2\bar{v}_3) + \gamma(v_2^2 - \bar{v}_2^2) + \cdots. \tag{27}$$

Therefore, it does not matter whether $\{v_2,v_3\}$ are both real or both imaginary, $\dot{\xi}_0 = \dot{\varphi} = 0$, and there will no traveling waves, i.e., rolls cannot drift.

In the complementary eigenspace $A_2' = A_3' = 0$, we can write (22a) as

$$\dot{A}_1 = \alpha A_1 + \beta A_4\bar{A}_1 + \gamma A_1^3\bar{A}_4 + O(|A|^5), \tag{28}$$

where the coefficients are functions of the invariants $|A_j|^2$, $j=1,4$. But now, $A_1 = |A_0|\exp i\xi_0 + |A_1'|\exp i\xi_1'$, and the spans of the two eigenspaces C_1 and C_2 require separate treatment. On C_1 the invariant v_1 is real, thus implying $\xi_1' = \xi_0$, and $A_1 = |A_1|\exp i\xi_0$. Now, from (28), by using the definition $\dot{\varphi} := \dot{A}_1\bar{A}_1 - A_1\dot{\bar{A}}_1 = 2i|A_1|^2\dot{\xi}_0$ together with the previous expressions for the amplitudes, we find for the phase velocity $\dot{\xi}_0 = \dot{\varphi} = 0$. Therefore, no propagation is possible.

On the span of C_3 the invariant v_1 is imaginary, thus implying $\xi_1' = \xi_0 + \pi/2$ and $A_1 = (|A_0| + i|A_1'|)\exp i\xi_0$. In addition, v_4 is also imaginary, thus $A_4' = i|A_4'|\exp 2i\xi_0$. By including both expressions in (28), we obtain for the real part

$$\dot{\xi}_0 = -(\beta + 3\gamma|A_0|^2)|A_4'| - \alpha_1|A_0||A_1'| + \cdots, \tag{29}$$

where we have used the fact that the unperturbed solution of (28) is given by $\alpha = \alpha_0 + \alpha_1|A_0|^2 + \cdots = 0$.

The implication of (29) is that $\dot{\xi}_0 \neq 0$ and traveling waves are possible. The second member of (29) is a function of the amplitudes, which, if they destabilize as a Hopf bifurcation, result in an oscillating phase speed. Therefore, the bifurcation preserving $S_1\times S_2\times S_3$, can destabilize reversing traveling waves.[15] The phase ξ_0 can be computed near the bifurcating point by taking $v_4 = v_{40}\cos\omega t$, from which

$|A_4'|=A\cos\omega t$ and (29) integrates to $\xi_0=\xi_{00}\sin\omega t$, with $\xi_{00}=-A\omega^{-1}(\beta+3\gamma|A_0|^2)$, thus giving an oscillatory phase to the roll.

We shall now write from (18) explicit expressions of T' for each family of solutions. We could also write an expression for χ' by noticing that $\partial_x\chi'$, like T', is a scalar field, so that they both display the same functional structure. The S_1-invariant solutions can be written as

$$T'=[T_0C_0(z)+T_2\cos\omega tS_1(z)]\cos kx + T_3\cos(\omega t+\vartheta)C_2(z)\cos 2kx+\cdots \quad (30)$$

which corresponds to a standing wave. And the $S_2\times S_3$-invariant solution reads

$$T'=T_0C_0(z)\cos kx+T_2\cos\omega tS_1(z)\sin kx + T_3\cos(\omega t+\vartheta)C_2(z)\sin 2kx+\cdots \quad (31)$$

which is a standing wave on top of the steady roll. The structure of the solutions invariant against the full group G of symmetries can be written as

$$T'=[T_0C_0(z)+T_1\cos\omega tC_1(z)]\cos kx + T_4\cos(\omega t+\vartheta)S_2(z)\cos 2kx+\cdots \quad (32)$$

which is again a standing wave. Finally, the bifurcation of $S_1\times S_2\times S_3$-invariant solutions gives

$$T'=T_0C_0(z)\cos[kx+\xi_0(t)]+T_1C_1(z)\cos(\omega t+\vartheta)\times\sin[kx+\xi_0(t)]+T_4S_2(z)\cos\omega t\times\sin 2[kx+\xi_0(t)]+\cdots . \quad (33)$$

This is a traveling wave with an oscillatory phase velocity $c=-k^{-1}\xi_{00}\sin\omega t$, which is linear in the amplitude of the perturbation, as can be seen from (29).

In order to validate the model, we have checked that the symmetries in (30)–(33) agree with the symmetries displayed by the numerical solutions, i.e., in the expansions (7) for these solutions, the appropriate coefficients are zero. To be more precise, near the secondary bifurcation the numerical results show that the dominant terms are the ones in the previous expressions, except for the roll mode, $T_0C_0(z)\cos kx$, which models the primary flow and should include two or three non-negligible overtones. This is why (22) is a model and not an asymptotically valid system, indeed. We have also carefully checked that the numerical results support the standing waves (30)–(32). In what concerns the traveling waves (33), no numerical support can be provided because this bifurcation has never been found to be dominant—see Fig. 1.

V. CONCLUSIONS

In the present paper we have shown that large-scale flows can be destabilized by resonant processes in many ways. We have examined the instability and dynamics of a single pair of rolls in a periodic domain. At onset the flow can break reflection symmetry S_1 by shearing the cross section of the roll, which results in a large-scale flow of antisymmetric velocity profile, or through a deformation of the cross section, which gives rise to a symmetric velocity profile, though the latter case has never been found to be dominant. At larger Rayleigh numbers every symmetry breaks down, the solution becomes chaotic and a large-scale flow is destabilized. These regimes are associated with a net mass flux, and this is important because they can be killed or strongly distorted by forcing the net mass flux to be zero, a constraint that is often imposed in streamfunction formulations by the boundary conditions.

We have computed the marginal stability curves and the sequence of symmetry breaking bifurcations for a pair of rolls in a periodic channel. The system always produces temporal chaos as a final stage, with the whole dynamics being confined to a low-dimensional manifold. For the Prandtl number value examined, the large-scale flow bifurcates by tilting the cross section of the cells only in small aspect ratio containers. If the aspect ratio is intermediate the large-scale flow bifurcates as a chaotic regime with no spatial symmetry. The Rayleigh numbers for such a bifurcation decrease with the aspect ratio. For containers of aspect ratio $L\simeq 6$, these flows destabilize for Rayleigh numbers $R\simeq 1.6\times 10^4$, well within the experimental range. Whether such resonant processes will survive in 3-D experiments, where the background is expected to be turbulent,[1] is still a challenging question.

We have concentrated our efforts on the simulation of convection in three small aspect ratio containers. If the dynamics of a system made of n pairs of rolls could be obtained by replicating n times a system made of a pair of rolls, the three examples that we have examined in this paper would describe the dynamics of every system with Prandtl number values $\sigma\simeq 10$. However, other resonances are expected to play an important role, thus reducing the scope of the present results. The dynamics of a one pair of rolls system has also been examined by using a low-dimensional model derived by a formal theoretical group technique. It shows that every one of the bifurcations that we have found numerically is a Hopf bifurcation associated with a (1:1:2) resonance, thus explaining the failure of previous models to describe their dynamics. It also shows that neither of the dominant bifurcations can lead to traveling waves but, in contrast, traveling waves could well be destabilized for the solutions with a symmetric mean velocity profile. To be precise, these are waves with an oscillatory phase, thus reversing periodically the sense of propagation. This oscillatory dynamics for roll patterns has been found elsewhere by using nonlinear phase dynamics.[18] Thus drifting rolls could be the outcome of plain convection in a convenient range of parameters. Migration of rolls has been reported from experiments in low Prandtl number fluids.[3]

The system described in this paper belongs to a family of problems that has received much attention in recent times. For many of these systems, breaking reflection symmetry S_1 is a sufficient condition to trigger traveling waves. This is the case, for instance, in compressible convection or magnetoconvection,[19] but as shown in Sec. III C, breaking reflexion symmetry may not be enough to destabilize traveling waves in 2-D systems. A similar conclusion was reached in Ref. 20. The Boussinesq system described in the present paper shows up–down symmetry, which is a requirement for

$S_2 \times S_3$ invariance, and such invariance constrains the system as much as S_1 does. This can be seen from (27), where the $S_2 \times S_3$ symmetry imposes a constant value on the translation phase, thus precluding traveling waves.

The geometry and dynamics obtained for the smaller aspect ratio container $L = 1$ is consistent with some recent results obtained elsewhere[6] for stress-free boundaries and small Prandtl number $\sigma = 1$. There is a minor difference, however, because the bifurcation reported there is steady but followed by a tertiary bifurcation of Hopf type. Unfortunately, the terminology used by the author is misleading. For instance, what he calls a "linear stability diagram"—see his Fig. 5—should, in our terminology, be termed a Reynolds number versus Rayleigh number diagram, with the former being defined $\mathrm{Re} := U_{\max}/\sigma$. The amplitude $U_{\max}$ is not an externally imposed parameter and should not be used to describe the stability of the flow. Difficulties come from his posing an initial value problem, which may not be the best strategy for exploring the dynamics of a flow with external forcing.

Experiments are very scarce and somewhat challenging. The periodic tilting of the cells observed in the large aspect ratio experiment quoted above[3] certainly stresses the confidence in our results, but the bifurcation reported for the aforementioned Hele–Shaw cell experiments[2] is steady, even though the Prandtl numbers for theory and experiments are similar. The fact that the latter experiment was conducted in a container with different top and bottom boundaries, thus breaking up–down symmetry, does not help comparisons. But it is worthwhile to recall that in none of the numerical simulations of convection in compressible fluids, i.e., with broken up–down symmetry, a reversal of the mean flow was reported[4,5], thus showing that the bifurcations were not of Hopf type. If the system is not $S_2 \times S_3$ symmetric, only the reflection symmetry S_1 remains, and this constraint may not be enough to force the resonances driving our system.

ACKNOWLEDGMENTS

It is a pleasure to acknowledge fruitful discussions during the course of the present work with Dr. E. Knobloch. One of us (J. M. M.) thanks the Department of Physics of the University of California at Berkeley for hospitality during a sabbatical leave, and J.P. acknowledges support from a CIMNE fellowship. We have received financial support from DGICYT, Spain, under Grant Nos. PB91-0595 and 92-203, and a CESCA grant for numerical computation.

[1] R. Krishnamurti and L. N. Howard, "Large-scale flow generation in turbulent convection," Proc. Natl. Acad. Sci. **78**, 1985 (1981).
[2] L. N. Howard and R. Krishnamurti, "Large-scale flow in turbulent convection: a mathematical model," J. Fluid Mech. **170**, 385 (1986).
[3] G. E. Willis and J. W. Deardorff, "The oscillatory motions of Rayleigh convection," J. Fluid Mech. **44**, 661 (1970).
[4] N. E. Hurlburt, J. Toomre, and J. M. Massaguer, "Two-dimensional compressible convection extending over multiple scale heights," Astrophys. J. **282**, 557 (1984).
[5] G. P. Ginet and R. N. Sudan, "Numerical observations of dynamic behavior in two-dimensional compressible convection," Phys. Fluids **30**, 1667 (1987).
[6] J. M. Finn, "Non-linear interaction of Rayleigh–Taylor and shear instabilities," Phys. Fluids B **5**, 415 (1993).
[7] J. M. Massaguer, E. A. Spiegel, and J. P. Zahn, "Convection-induced shears for general planforms," Phys. Fluids A **4**, 1333 (1992).
[8] F. H. Busse and A. C. Or, "Subharmonic and asymmetric convection rolls," J. Appl. Math. Phys. **37**, 608 (1986).
[9] D. Armbruster, "O(2)-Symmetric bifurcation theory for convection rolls," Physica D **27**, 433 (1987).
[10] J. Mizushima and K. Fujimura, "Higher harmonic resonance of two-dimensional disturbances in Rayleigh–Bénard convection," J. Fluid Mech. **234**, 651 (1992).
[11] J. M. Massaguer, "Shear type instabilities in the Benard Problem," in *The Global Geometry of Turbulence*, Advanced Nato Series, edited by J. Jiménez (Plenum, New York, 1991), Vol. 247.
[12] I. Mercader, M. Net, and A. Falqués, "Spectral methods for high order equations," Comp. Meth. Appl. Mech. Eng. **91**, 1245 (1991).
[13] J. Prat, I. Mercader, and J. M. Massaguer, "Symmetric large-scale velocity fields in 2-D thermal convection," Int. J. Bifurcation Chaos (in press, 1994).
[14] J. Prat, J. M. Massaguer, and I. Mercader, "Mean flow in 2-D thermal convection," *Mixing in Geophysical Flow*, edited by J. M. Redondo and O. Metais (UPC, Barcelona, in press).
[15] A. S. Landsberg and E. Knobloch, "Direction-reversing traveling waves," Phys. Lett. A **159**, 17 (1991).
[16] J. D. Crawford and E. Knobloch, "Symmetry and symmetry-breaking bifurcations in fluid dynamics," Annu. Rev. Fluid Mech. **23**, 341 (1991).
[17] E. Knobloch and J. Guckenheimer, "Convective transitions induced by a varying aspect ratio," Phys. Rev. **27**, 408 (1983).
[18] J. M. Massaguer, "Large-scale flow and pattern drift in finite amplitude convection," Phys. Fluids **7**, 2304 (1994).
[19] P. C. Matthews, M. R. E. Proctor, A. M. Rucklidge, and N. O. Weiss, "Pulsating waves in non-linear magnetoconvection," Phys. Lett. A **183**, 69 (1993).
[20] E. Knobloch, "Bifurcations in rotating systems," in *Theory of Solar and Stellar Dynamos: Introductory Lectures*, edited by M. Proctor and A. Gilbert (Cambridge University Press, Cambridge, 1993), Chap. 11.